

ARTERIAL IMAGING

Accuracy of Quantitative MR Vessel Wall Imaging Applying a Semi-Automated Gradient Detection Algorithm—A Validation Study

Qian Wang,[#] Matthew D. Robson,[#] Jane M. Francis, Steffen E. Petersen,
Keith M. Channon, Stefan Neubauer, and Frank Wiesmann, M.D.*

University of Oxford Center for Clinical Magnetic Resonance Research, Department
of Cardiovascular Medicine, University of Oxford, Oxford, UK

ABSTRACT

Magnetic resonance imaging (MRI) is uniquely suited to study the pathophysiology of arteriosclerosis. So far, magnetic resonance (MR) measurements of vessel dimensions have mainly been done by manual tracing of vessel wall contours. However, such data postprocessing is very time-consuming and has limited accuracy due to difficulties in precise tracing of the thin vessel wall. *Purpose:* To assess the accuracy and reproducibility of quantitative vascular MR imaging applying a data analysis method based on (1) vessel wall unwrapping, followed by (2) a gradient detection algorithm for MR data postprocessing. Vascular MR imaging studies were done both in vessel phantoms and in healthy volunteers ($n=29$) on a clinical 1.5 T MR scanner. A dark blood double-inversion turbo spin echo sequence with fat suppression was applied, with proton-density-weighted and breath-hold acquisition for aortic imaging and T2-weighted acquisition for carotid imaging. Intraobserver and interobserver variability were systematically evaluated by two independent observers. A repeat study within 10 days of the first MRI was performed in 10 of these subjects for assessment of interstudy reproducibility. *Results:* The semiautomated edge detection software revealed a clear view of the inner and outer vessel wall boundaries both in the phantoms and in the volunteers studied. There was close agreement between MR-derived measurements and phantom dimensions (mean difference of $1.1 \pm 16.9 \text{ mm}^2$, $8.0 \pm 19.9 \text{ mm}^2$, $9.0 \pm 12.1 \text{ mm}^2$ for vessel wall cross-sectional area, inner vessel area, and total vessel area, respectively). Quantification of vessel dimensions was feasible in all 29 healthy volunteers studied. Semiautomated quantification of cross-sectional vessel wall area (mean \pm SD, $253.6 \pm 208.4 \text{ mm}^2$) revealed close correlation for repeated measurements by one or two observers ($r=0.99$ each). Both intraobserver

[#]Both authors contributed equally to this manuscript.

*Correspondence: Frank Wiesmann, M.D., Experimentelle Physik (EP5), Physikalisches Institut, Universität Würzburg, Am Hubland, 97074 Würzburg, Germany; Fax: +49-931-888-5508; E-mail: f.wiesmann@mail.uni-wuerzburg.de.

and interobserver variability of vessel wall area MR measurements were low (mean difference $7.5 \pm 16.7 \text{ mm}^2$ and $14.4 \pm 24.6 \text{ mm}^2$, respectively). In the repeat study of 10 volunteers, MRI with semiautomated postprocessing quantitation revealed a high correlation and agreement of vessel dimensions between the two scans ($r=0.994$, mean difference $2.6 \pm 25.1 \text{ mm}^2$). *Conclusion:* Semiautomated analysis methods can provide approaches that benefit from the human understanding of the image and the computer's ability to measure precisely and rapidly. Thus, by combining the latest MRI methods and semiautomated image analysis methods, we are now able to reproducibly determine the geometric parameters of blood vessels.

Key Words: Vascular imaging; Black blood MRI; Vessel wall area; Postprocessing; Edge detection; Quantitative MRI; Reproducibility.

INTRODUCTION

Atherosclerosis resulting in ischemic cardiovascular events such as myocardial infarction or stroke is the leading cause of mortality in adults (Ross, 1999). The severity of arteriosclerosis may be determined by visualizing luminal stenosis and changes in vessel wall structure. In terms of predicting clinical risk, assessment of luminal stenosis alone is insufficient, as during early stages of arteriosclerotic plaque formation, vessel remodeling and plaque growth can occur without compromising luminal size (Glagov et al., 1987). Previous trials have demonstrated that luminal narrowing in the carotid arteries is only of limited value in predicting plaque vulnerability and stroke (North American Symptomatic, 1991).

In order to visualize atherosclerotic changes both in peripheral and, even more importantly, in central arteries such as the coronaries or the carotid arteries, a variety of different imaging techniques such as X-ray angiography, external ultrasonography, and, more recently, intravascular ultrasound imaging have been developed (Cao et al., 2003; Rewis et al., 2003; Sahara et al., 2003; Wu et al., 2003). However, these techniques are either invasive and thus not suited for routine clinical follow-up or suffer from restrictions such as pure luminography of X-ray angiography or high operator dependency of ultrasound imaging (Montauban van Swijndregt et al., 1999).

Magnetic resonance imaging (MRI) is a noninvasive technique that provides high image resolution and excellent soft-tissue contrast. MRI has advantages over alternative imaging modalities in visualizing the arterial wall and may play an increasingly important role in the research of atherosclerotic lesion formation. Previous work has demonstrated the ability of MRI to characterize the composition of both in vivo and ex vivo human atherosclerotic plaques (Shinnar et al., 1999; Toussaint et al., 1996; Yuan et al., 2001). Particularly, high-resolution black-blood MRI techniques

with multiple contrast weightings proved useful in quantitative assessment of arterial plaque area and total plaque burden (Fayad et al., 2000a,b; Yuan et al., 1998; Zhang et al., 2001).

At present, quantitative measurements of various vascular parameters such as wall thickness and cross-sectional area, luminal area, and plaque volume are being performed by manual tracing of the inner and outer vessel wall boundaries of the MR images. Due to the rather small arterial wall compartment in comparison to the larger luminal compartment, these manual delineations introduce a certain degree of error to the quantitative vessel dimension analysis. Furthermore, manual contour tracing makes the data postprocessing subjective, highly labor intensive and time-consuming.

Hence, to study the dynamics of arteriosclerosis development and to noninvasively evaluate the effects of new therapeutic strategies, more reproducible ways of data analysis for quantification are needed. Suitable postprocessing algorithms would facilitate the data evaluation process and may significantly reduce operator subjectivity.

The purpose of this study was to assess the feasibility, accuracy, and reproducibility of quantitative vascular MR imaging, applying a measurement method based on unwrapping the vessel wall followed by a gradient detection algorithm for data postprocessing of both phantom and volunteer vessel studies. We hypothesized that a standardized semiautomated postprocessing algorithm can reduce data analysis time and provide accurate and reproducible measurements of vascular dimensions.

MATERIALS AND METHODS

Phantom Study

For validation of vessel dimension quantification, a vessel phantom was built of synthetic glass, consisting

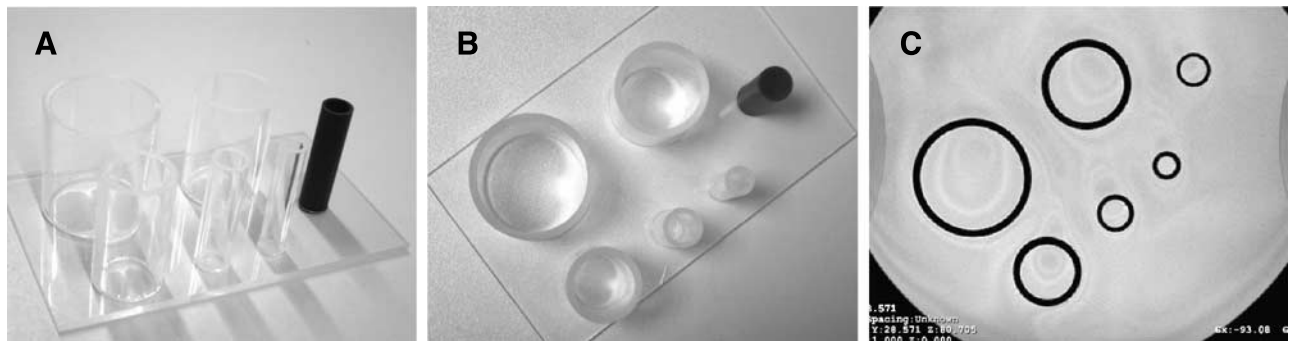


Figure 1. Vessel-phantom for validation of quantitation accuracy using a semiautomated edge detection postprocessing algorithm. Phantom viewed from (A) oblique and (B) above. (C) Corresponding MR turbo spin-echo image visualizing the six synthetic glass tubes.

of six tubes of varying size and wall thickness corresponding to features of human aorta and carotid arteries (inner diameter range 8.05 mm to 44.07 mm, wall thickness range 1.56 mm to 3.09 mm, measured by a sliding caliper). These tubes were mounted orthogonally on a synthetic glass plate to ensure correct MR image plane alignment perpendicular to the tubes. For MR imaging, the phantom was put into a water tank to provide sufficient contrast between the tubular walls and their surroundings (Fig. 1).

Volunteer Study

Twenty-nine healthy volunteers (16 males, mean age 33.8 ± 8.2 years, range 23–62 years) with and without cardiovascular risk factors were studied. Black blood MRI was performed in the thoracic aorta and in the carotid arteries of all subjects studied. Intraobserver reproducibility of data evaluation was assessed for the entire study population. Interobserver variability was

evaluated from 17 MR studies randomly chosen. In 10 subjects, a repeat study within 10 days of the first MRI was performed for assessment of interstudy reproducibility. All subjects gave informed consent, and the study was approved by the Local Research Ethics Committee (Fig. 2).

MR Imaging

All studies were performed on a 1.5 T clinical MR scanner (Siemens Sonata, Erlangen, Germany) with a gradient performance of 40 mT/m and a slew rate of 200 T/m/s.

Volunteers were scanned in supine position, and four-lead ECG signals were used for triggered MR data acquisition. For aortic imaging, a two-channel flexible-array chest coil was used combined with two elements of the spine array coil. Transverse Half-Fourier acquisition single-shot turbo spin echo (HASTE) images in transverse and oblique sagittal orientation

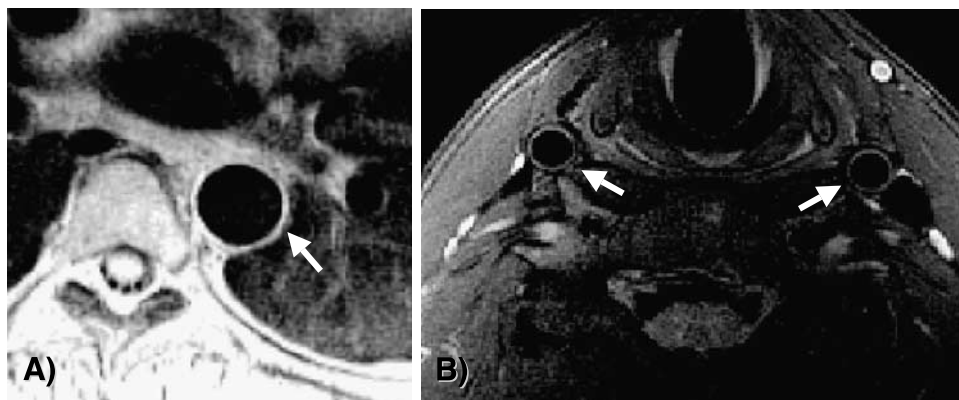


Figure 2. Dark blood turbo spin echo MR image of (A) thoracic descending aorta and (B) both common carotid arteries (images cropped for display purposes).

were acquired for localization of the aortic arch. Based on these, proton-density-weighted (PDW) transverse double-inversion turbo spin echo (TSE) images with a 180° preparation pulse for black blood imaging and fat suppression were acquired. A series of seven transverse slices of the descending aorta were acquired, starting from the level of pulmonary artery bifurcation, with slice thickness of 5 mm, field of view (FOV) 200×200 mm, matrix 256×256 , and in-plane resolution of 0.8×0.8 mm. For proton density weighting, echo time (TE) was 11 ms, and repetition time (TR) equaled one R–R interval. Data acquisition was triggered to the R-wave in every cardiac cycle and 19 cardiac cycles were acquired for each slice.

For carotid imaging, a pair of soft two-channel coils customized for neck vessel imaging (Machnet, the

Netherlands) were used, positioned on both sides of the neck. Due to variations in carotid bifurcation level in individuals, adjustments of coil position were made where necessary to gain optimal MR signal from the carotid arteries. The carotid bifurcation was illustrated by an axial three-dimensional (3D) time of flight (TOF) imaging scout, and the central slice of a TSE sequence was chosen at 1 cm below the lower bifurcation of either side of the carotid arteries. Double-inversion turbo spin echo images with T2-weighting (T2W) and fat suppression were acquired without breath-holding. MR imaging parameters were as the following: FOV 150×150 mm, matrix 320×320 , in-plane resolution 0.5×0.5 mm, slice thickness 3 mm, TR equally 2 RR-intervals, and TE 81 ms. Five to seven contiguous slices were acquired. Data acquisition was triggered on every second

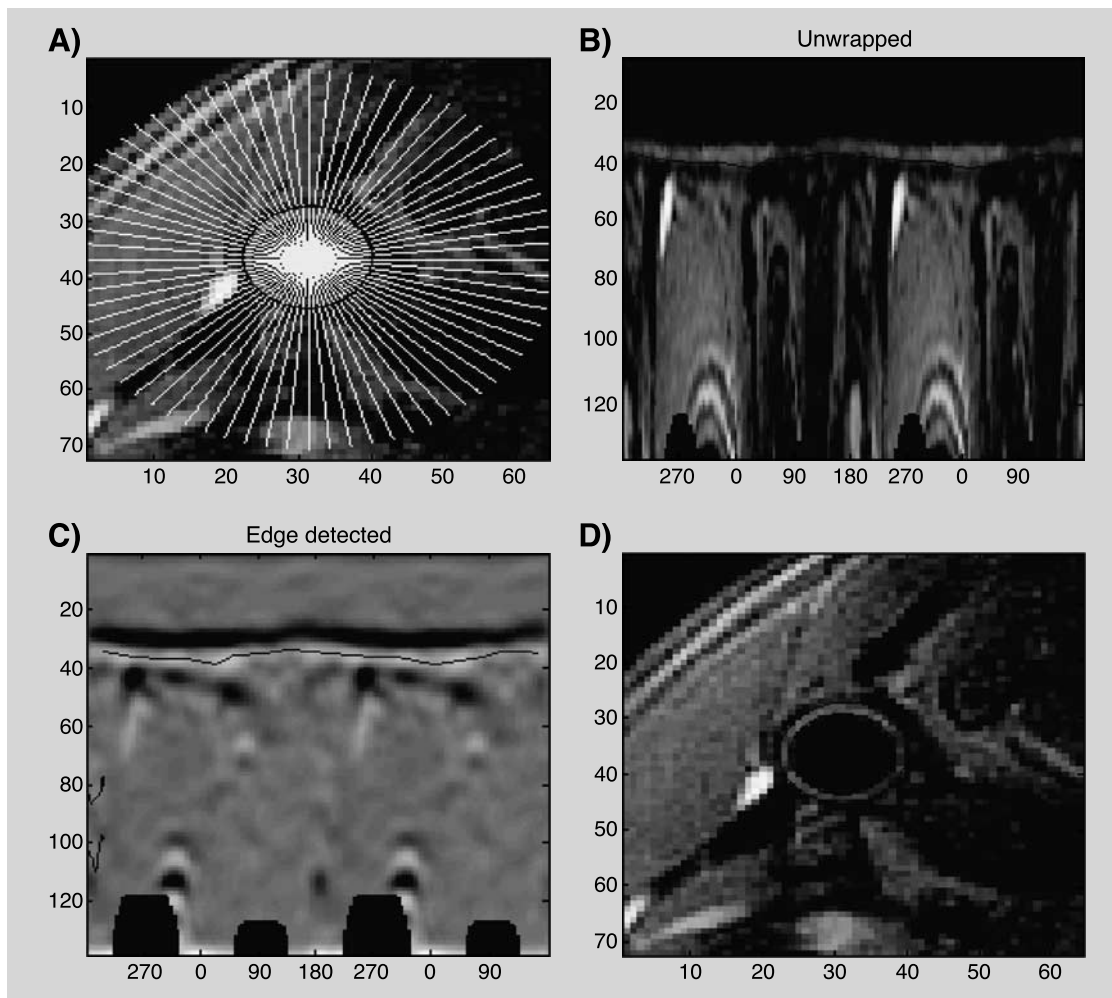


Figure 3. Results of the edge detection analysis showing (A) reference lines for carotid vessel wall profile, (B) “unwrapped” image data, (C) result of gradient-detection for inner (black) and outer (white) wall boundaries (with suggested outer edge segmentation superimposed as black line), and (D) visual display of segmentation result (black lines).

heartbeat and 36 cardiac cycles were acquired for each slice.

For the phantom study, two elements of the spine-array coils were used. Data acquisition was triggered by an external electronic trigger unit set to a frequency of 60/min. Applying PDW TSE imaging, one transverse slice was acquired with identical parameters to the aortic imaging protocol.

Image Analysis

The semiautomated quantitation analysis method was implemented under Matlab (Version 6.5, The Mathworks, Inc., Natick, MA) and was run on a standard PC. The implementation performed two computerized steps: (1) the vessel wall was “unwrapped” with the manually defined center of the vessel, which was performed by first interpolating the image (four times in each direction using cubic interpolation) and then mapping the pixel intensities into the polar coordinates of the vessel. Each interpolation and remapping stage will degrade the image quality, and so by “over-interpolating” in this way we avoid further degradation by the subsequent remappings.

The mapping into polar coordinate space first determines an approximate center of mass of the vessel from user input points on the boundary of the vessel. Subsequently, linear interpolation is used to calculate the image intensity along each of a number of rays propagating from this center of mass, data are calculated for two complete rotations so that the subsequent segmentation is insensitive to the choice of starting angle. This mapping into polar coordinates is designed so that spatial distortions are minimized at the radius of the vessel.

(2) Gradient determination was achieved by an edge detection filter in the radial direction, which smoothed in the angular direction while differentiating in the radial direction. This filter was optimal with respect to the Canny criteria (Canny, 1986), which could be performed in the polar coordinate space.

Following the above steps, the user was able to position points that were maxima (for the lumen/inner vessel wall interface) or minima (for the outer vessel wall/peripheral tissue) in the gradient image. Determination of these points did not require a gray-level decision to be made, and the user only positioned points (typically, 15 points per vessel) where the boundary location was clear. The computer then interpolated between those points in the polar coordinate space, which had the benefit of joining the points with smooth curves and hence operated well even when a small number of boundary points had been defined. This procedure

was performed for both the inner and outer vessel wall boundary. The contours suggested by the algorithm were visually displayed (Fig. 3). If the user was not satisfied with the inner or outer wall delineation, remeasurement was possible by correction of the set boundary points. Once wall delineation was completed, the program returned the total vessel area, the lumen area, and the wall area as well as the mean, maximum, and minimum wall thickness in each image plane. All data were saved as ASCII text files and were exported to Excel spreadsheets for further parameter calculations.

Accuracy and Reproducibility Assessment

To assess the accuracy of the quantification algorithm, segmentation results of MR-derived phantom parameters such as cross-sectional vessel wall area, total vessel area, and luminal vessel area were compared with the corresponding true phantom dimensions.

Intraobserver and interobserver variability were systematically evaluated by repeated MR data analysis by one observer (A1 vs. A2) and by two independent observers (A vs. B), respectively. For assessment of interstudy variability, MR images of the repeated studies of 10 subjects (S1 vs. S2) were also analyzed by observer A.

Statistical Analysis

All statistical analyses were performed using StatView (Version 5, SAS Institute). Total cross-sectional vessel area and luminal vessel area were assessed from the regions of interest given by the semiautomated segmentation process. Vessel wall cross-sectional area was calculated as the difference between total and luminal vessel area. Furthermore,

Table 1. Absolute and relative differences between MR-derived and true phantom vessel dimensions.

	Absolute difference (true MR-derived dimensions), mm ²	Relative difference (true MR-derived dimensions), %
Phantom wall area	9.0±12.1	2.0±3.9
Phantom inner area	-7.9±19.8	-1.0±2.6
Phantom total area	1.0±16.8	-0.1±2.6

Data are given as mean±SD.

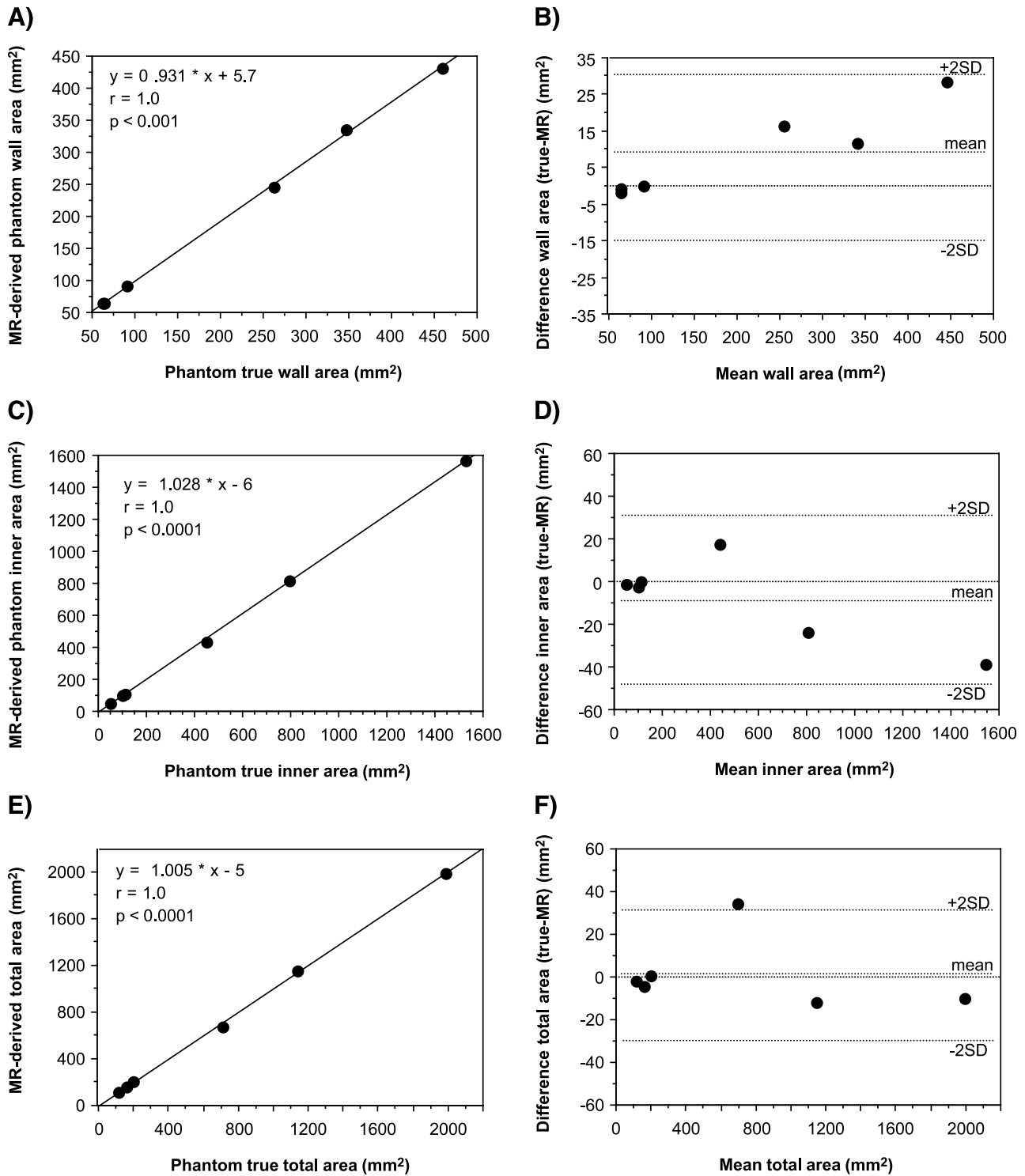


Figure 4. Results of phantom study for vessel-dimension quantitation validation. Note the high correlation between MR-derived measurements for (A) wall area, (C) inner phantom area, and (E) total phantom area with true phantom dimensions. Parts (B), (D), and (F) show the corresponding Bland-Altman plot for assessment of measurement agreement.

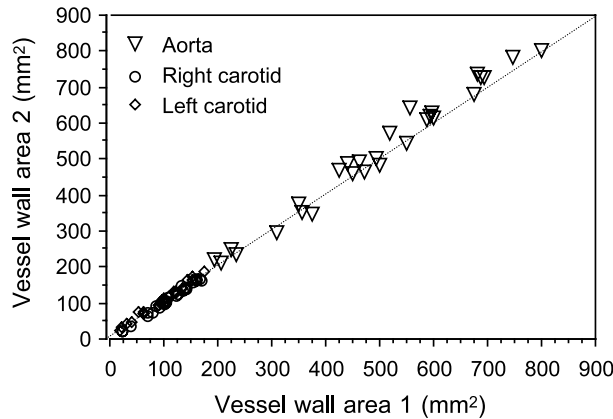


Figure 5. Repeated measurement of cross-sectional vessel wall area by semiautomated MR image quantification analysis (dotted line represents line of identity).

vessel wall thickness in each image analyzed was given as mean, maximum, and minimum value per slice measured. Total cross-sectional vessel wall area of each vessel was calculated from all slices analyzed. Simple linear regression analysis was performed to characterize degree of correlation between postprocessing analysis results and true dimensions. Reproducibility of repeated data analysis and MR measurements was evaluated by calculation of absolute and relative differences between measurements. Overall agreement of repeated measurements was assessed by Bland-Altman analysis. A p -value of <0.05 was considered statistically significant.

RESULTS

Phantom Measurements

MR images of the vessel phantom revealed high contrast between the low signal of the plastic tubes and the high-intensity water background (Fig. 1B). The lumen/inner wall interfaces and the outer wall/surrounding water interfaces were clearly distinguished by the semiautomated edge-detection algorithm. Com-

parison of MR measurement results and true phantom dimensions showed no differences for vessel wall cross-sectional area ($205.6 \pm 156.4 \text{ mm}^2$ vs. $214.6 \pm 167.8 \text{ mm}^2$, $p=0.13$), inner vessel area ($513.3 \pm 591 \text{ mm}^2$ vs. $505.3 \pm 575.3 \text{ mm}^2$, $p=0.37$), and total vessel wall area ($718.9 \pm 742.5 \text{ mm}^2$ vs. $719.9 \pm 738.3 \text{ mm}^2$, $p=0.89$). There was close agreement between MR-derived measurements and phantom dimensions (mean absolute differences $9.0 \pm 12.1 \text{ mm}^2$, $-8.0 \pm 19.9 \text{ mm}^2$, and $-1.1 \pm 16.9 \text{ mm}^2$ for vessel wall cross-sectional area, inner vessel area, and total vessel area, respectively). Relative differences between MR-measurements and true phantom dimensions were $2.0 \pm 3.9\%$, $-1.0 \pm 2.6\%$, and $-0.1 \pm 2.6\%$ for vessel wall cross-sectional area, inner vessel area and total vessel area, respectively (Table 1). Correlation of MR-derived measurements and true vessel wall dimensions in all phantoms was high ($r=1.0$, MR-derived wall area = $0.931 * \text{true wall area} + 5.7 \text{ mm}^2$, $p < 0.001$) (Fig. 4). Furthermore, there was a close correlation between MR results and true phantom dimensions for both cross-sectional inner area ($r=1.0$, MR-derived wall area = $1.028 * \text{true wall area} - 6.0 \text{ mm}^2$, $p < 0.0001$) and total vessel phantom area ($r=1.0$, MR-derived wall area = $1.005 * \text{true wall area} - 5.0 \text{ mm}^2$, $p < 0.0001$).

Volunteer Study

Quantification of vessel dimensions applying the semiautomated edge detection method described was performed in all subjects studied. In general, the image plane encompassing the site of carotid bifurcation has been excluded from data analysis, since the algorithm cannot provide a correct unwrapping when the vessel lumen is oblong. Quantitative MR data analysis was hampered in part in three subjects studied due to motion and susceptibility artifacts resulting in reduced overall image quality. In these subjects, definition of inner and outer vessel borders was limited. When applying the semiautomated edge detection algorithm to these data sets, areas of blurred boundaries were omitted during computer-assisted manual edge definition, but were interpolated from the set data points. After visual control of the suggested boundaries, the

Table 2. Absolute (and relative) intraobserver, interobserver, and interstudy variability of repeated MR measurements of cross-sectional vessel wall area in volunteers applying semiautomated postprocessing.

	Intraobserver variability (n=29)	Interobserver variability (n=17)	Interstudy variability (n=10)
Aorta	$11.1 \pm 25.1 \text{ mm}^2$ ($2.0 \pm 5.4\%$)	$30.5 \pm 34.6 \text{ mm}^2$ ($7.2 \pm 9.5\%$)	$4.9 \pm 26.9 \text{ mm}^2$ ($0.12 \pm 5.6\%$)
Carotid arteries	$2.7 \pm 5.2 \text{ mm}^2$ ($2.4 \pm 5.7\%$)	$5.2 \pm 7.4 \text{ mm}^2$ ($4.8 \pm 7.7\%$)	$-1.3 \pm 4.6 \text{ mm}^2$ ($-1.0 \pm 6.7\%$)
Overall	$5.5 \pm 15.6 \text{ mm}^2$ ($2.3 \pm 5.6\%$)	$14.4 \pm 24.5 \text{ mm}^2$ ($5.6 \pm 8.4\%$)	$1.4 \pm 17.8 \text{ mm}^2$ ($0.49 \pm 6.1\%$)

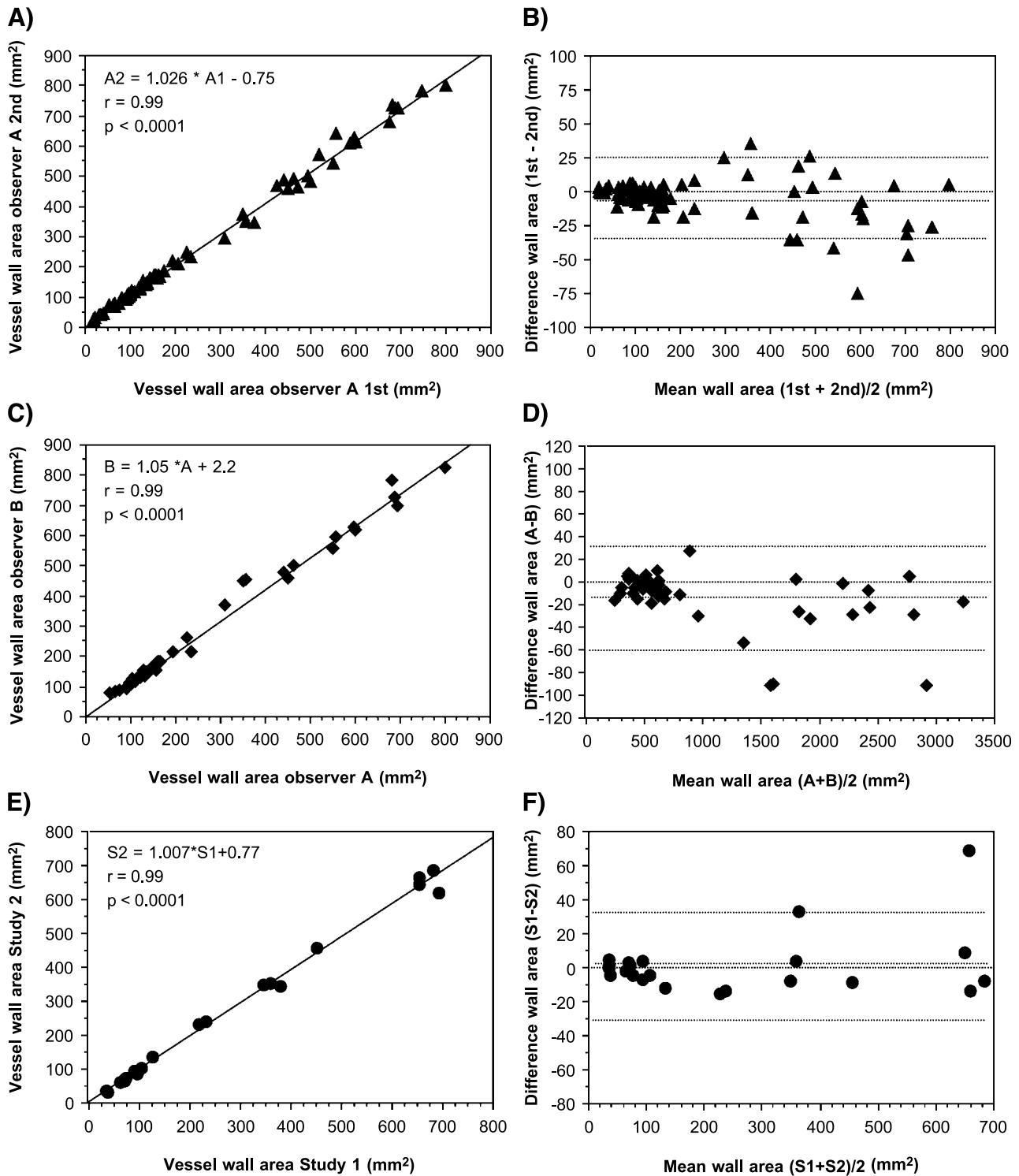


Figure 6. Correlation of repeated MR data analysis by semiautomated postprocessing for (A) intraobserver, (C) interobserver, and (E) interstudy comparisons. Parts (B), (D), and (F) reveal the corresponding Bland-Altman plots for measurement agreement, respectively.

segmentation result was acceptable in two cases. In one volunteer, software-based border definition was rejected and the data set was excluded from quantitative analysis. In all the other images acquired, inner and outer vessel boundaries were correctly assigned by the gradient-detection algorithm, allowing precise boundary delineation and vessel wall segmentation (Fig. 3). Hence, a total of 400 vessel sections were analyzed by the postprocessing method with generation of multiple regions of interest for each section for intraobserver, interobserver, and interstudy comparisons, resulting in an overall number of 1200 regions of interest for the combined analysis of the aorta and the carotid vessels.

Quantification of cross-sectional areas in the aorta revealed a mean vessel wall area of $495.5 \pm 168.1 \text{ mm}^2$. Aortic total area and inner area were $1759.4 \pm 644.0 \text{ mm}^2$ and $1263.9 \pm 484.0 \text{ mm}^2$, respectively. Results for wall area, total, and inner vessel area for the carotid arteries were $104.7 \pm 41.7 \text{ mm}^2$, $293.9 \pm 121.0 \text{ mm}^2$, and $189.2 \pm 81.1 \text{ mm}^2$, respectively. Comparison of aortic vessel wall cross-sectional area and age revealed a close correlation ($r=0.49$, $p<0.01$), whereas there was no significant correlation of carotid wall area with age ($p=0.87$). However, carotid wall area correlated closely with volunteer height ($r=0.49$, $p<0.01$). Comparison of gender differences in vessel wall area showed significantly higher carotid wall areas in males compared to females (21.5 ± 0.6 vs. $19.3 \pm 0.6 \text{ mm}^2$, $p=0.03$), whereas comparison of aortic wall area did not reach statistical significance (117.4 ± 3.0 vs. $112.0 \pm 3.0 \text{ mm}^2$, $p=0.20$).

Intraobserver and Interobserver Variability

Semiautomated quantification of cross-sectional vessel wall area revealed close correlation for repeated data analysis by one observer (A1 vs. A2) ($r=0.99$, $A1=1.007 \cdot A2+0.77$). Similarly close correlations were found for the intraobserver comparison for total vessel area ($r=0.99$, $A1=1.007 \cdot A2+0.1$) and inner vessel cross-sectional area ($r=1.0$, $A1=1.002 \cdot A-0.2$) (Fig. 5). MR data analysis by two independent observers revealed correlation coefficients of 0.98, 0.99, and 0.99 for comparison of cross-sectional vessel wall area, total wall area, and inner wall area, respectively.

Furthermore, Bland-Altman analysis revealed close agreement of MR measurements of cross-sectional vessel wall area by observer A (mean difference $5.5 \pm 15.6 \text{ mm}^2$), and for comparison of observer A1 and B (mean difference $14.4 \pm 24.6 \text{ mm}^2$). Given the mean overall vessel wall area of $238.1 \pm 212.9 \text{ mm}^2$,

limits of agreement (analogical to ± 2 SD) for the Bland-Altman analysis were narrow both for intraobserver ($\pm 32.2 \text{ mm}^2$) and interobserver comparison ($\pm 49.2 \text{ mm}^2$). Hence, the maximal gradient detection method allowed for a high overall intraobserver and interobserver reproducibility for combined aortic and carotid MR imaging (Table 2).

Inter-Study Consistency

In the repeat study of 10 volunteers, 6 vascular sections of either the right or left carotid arteries were not feasible for the computer-aided analysis due to blurred MR images. Hence, a total of 24 vessels were available for quantitative post-processing analysis. A high correlation and interstudy agreement of vessel wall cross-sectional area was found at comparison between the repeated scans (S1 vs. S2) ($r=0.99$, $S1=0.98 \cdot S2+4.6$, $p<0.0001$). (Fig. 6E). Inter-study variability for separate comparisons of aorta and carotid arteries was $4.9 \pm 26.9 \text{ mm}^2$ for aortic and $1.3 \pm 4.6 \text{ mm}^2$ for carotid images. Bland-Altman analysis showed high overall agreement between the repeated studies (mean total difference of 1.43 mm^2 for cross-sectional vessel wall area) with narrow limits of agreement (Fig. 6F).

DISCUSSION

The results of our study yield two important findings: 1) Black blood MR images of central indicator vessels of arteriosclerosis such as the aorta or the carotid arteries can be analyzed using semiautomated gradient-detection postprocessing methods with high reproducibility. 2) The use of dedicated hardware such as phased-array surface coils and optimized imaging sequences for vessel wall imaging allows for high accuracy and robustness of quantitative MR imaging with subsequent semiautomated image analysis applying vessel-wall tracing algorithms. Hence, in addition to small intraobserver and interobserver variability indicated from repeated analysis of identical MR data sets, repeated MR studies also reveal high reproducibility of MR measurements of vascular dimensions.

This high interstudy reproducibility of quantitative vascular MRI is particularly important for monitoring patients with arteriosclerosis, since MR imaging may play a pivotal role in identifying new markers of plaque vulnerability. MRI has advantages over alternative imaging strategies by noninvasively providing high-resolution cross-sectional images of arteries, allowing for measurement of plaque cross-sectional

areas and plaque volumes. This is of major importance for clinical management of patients with arteriosclerosis, since recent clinical trials have impressively demonstrated lumen narrowing to be a poor predictor of plaque vulnerability (ACAS, 1994). However, accurate identification of vessel boundaries can be difficult due to certain signal features found in the vicinity of the vessel walls such as 1) insufficient contrast between blood, vessel wall and perivascular tissues; 2) contrast variations between normal and atherosclerotic vessel wall; and 3) image artifacts originating from blood flow and random patient motion (Yuan et al., 1999). All these considerations have to be dealt with by an ideal maximal gradient detection algorithm that should be robust enough to avoid misinterpretation of imaging artifacts for vessel walls. Furthermore, such a semiautomated algorithm should be able to generate images of various contrast and should allow for operator input and correction.

In this study, we demonstrate that a postprocessing method based on the principles of Canny edge detection (Canny, 1986) allows for highly accurate quantification of vascular dimensions from black blood MR images. The Canny approach is chosen because it provides a simple and easily implemented method that accurately localizes the edges and is designed to be insensitive to noise. Evaluation of measurements in a phantom study representing vessels with dimensions similar to those found in clinical MR studies of patients revealed an excellent agreement between MR data analysis results and true phantom dimensions.

With tubes mounted nonorthogonally, MR imaging would result in a slight overestimation of the vessel phantom wall thickness and total wall area, since semiautomated measurements in this study were based on an edge detection method. Hence, the partial volume effect would result in an increased wall thickness both at manual and semiautomated quantitative analysis. This is the main reason why exact orientation of the imaging plane relative to the vessel course is crucial to cut the vessel truly perpendicular and, thus, avoid this sort of measurement error.

Similarly, black blood MRI in volunteers using turbo-spin-echo sequences with fat-suppression prepulses provided robust image quality allowing for accurate tracing of vessel boundaries by the gradient-detection method. However, the algorithm has no potential of compensating for ghosting or motion artifacts sometimes present in carotid MR images. Since such artifacts may create the appearance of a false vessel wall boundary, it was crucial to crop the original MR images in order to focus only on the vessel of interest rather than its surroundings. Furthermore, the center of gravity within the inner vessel

boundary was defined by the algorithm, representing the starting point of the edge detection profile generation. In all cases, the suggested vessel boundary delineation given by the postprocessing algorithm was visually checked for plausibility. If there was misregistration due to ghosting artifacts, these errors had to be corrected manually. In the present study, the measurement accuracy is in close agreement with previous accuracy analysis of quantitative vascular MRI. Chan et al. (2001) demonstrated a high scan reproducibility of MR-based assessment of aortic atherosclerotic burden both in healthy volunteers and patients with coronary artery disease. In an MRI study in atherosclerotic patients, Corti et al. (2001) reported an accuracy of repeated MR studies of 5% and 7% for measurement of aortic and carotid vessel wall area.

Similar to previous studies, we were able to demonstrate a high correlation between aortic wall area and age (Li et al., 2004). Furthermore, there was a good correlation between carotid artery wall area and volunteer height. Comparison of gender differences in vessel wall area showed significantly higher carotid wall areas in males compared to females ($p=0.03$), whereas comparisons of aortic wall area remained below the significance level ($p=0.20$). This is most likely due to the relatively small sample size of this more methodological study.

Comparison to Other Edge Detection Methods

Various postprocessing algorithms have been tested for automatic contour tracking in medical images, including two-dimensional (2D) edge detection techniques in echocardiography images (Melton et al., 1983; Zhang and Geiser, 1984), fuzzy reasoning after edge detection (Feng et al., 1991), and morphologic edge detection (Klingler et al., 1988). The goal of these more complex approaches is generally to completely automate the segmentation procedure. Total automation is an interesting goal, but one that we do not seek. We believe that a semiautomated analysis approach will achieve the best result owing to its improved flexibility when image quality is poor, which it is always likely to be in some scans during practical clinical scanning. Important improvements in robustness of border tracing have been made by development of deformable (active) contour models ("snake" models) (Kass et al., 1988). The application of such algorithms to black blood MR images of the human carotid arteries showed a high sensitivity to contrast variations and proved highly accurate and reproducible for vessel cross-sectional area quantification (Berr et al., 1995; Yuan et al., 1999). We have not used the "snake" approaches;

although they appear to offer the best performance for automated approaches, they cannot be implemented in a semiautomated which we believe is essential for a robust scientific measurement tool.

Postprocessing Time vs. Analysis Accuracy

With any imaging modality, time efficiency of postprocessing is particularly crucial when large amounts of quantitative measurements from image data are needed. Here in lies the potential role of semiautomated algorithms to speed up this process and to avoid uneconomical use of human resources with tedious data analysis. The postprocessing time for tracing either the inner or outer boundary of one vessel in this study varied between 20 to 40 s, depending upon vessel anatomy and the overall image quality. Similarly, Yuan et al. (1999) reported a processing time in the range of 20 s to 2 min per vessel boundary. This indicates that, as yet, the semiautomated vessel wall segmentation is not significantly faster than manually tracing the vascular boundaries. This is particularly true in images with blurry or missing edges, where the operator has to interact with the segmentation algorithm and correct for algorithm misregistration of edges by manual adjustment of tracing points.

However, the main advantage of this method is that the combination of computer-driven feature extraction with operator-based manual corrections provides a significantly higher reproducibility of measurements. Since the algorithm provides the quantitative edge information, allowing operator interpretation that introduces variability only as necessary in difficult slices, it produces area measurements with high accuracy and very low variability. Yuan et al. (1999) reported of a high correlation between manual and algorithm-based measurements of luminal, total vessel, and vessel wall cross-sectional area with mean differences of 1.05 mm², 1.36 mm² and 0.31 mm², respectively. In a recent clinical study, Zhang et al. (2003) found a similar close correlation ($r=0.88$) for in vivo MR-results and ex vivo measurements postendarterectomy for quantifying carotid wall volume applying the snake algorithm.

Assessment of interobserver variability in this study showed a close correlation between the two blinded operators for quantifying total and luminal vessel area as well as vessel wall area ($r=0.99$ each). In a recent study, Weiss et al. (2001) also reported close correlation between two independent observers using computer-assisted image analysis ($r=0.88$). Their mean difference in wall thickness averaged 0.25 ± 0.28 mm, resulting in a coefficient of variation of 14%. In a study looking at accuracy of quantification of luminal

area in the carotid arteries of volunteers by the "snake" algorithm, Berr et al. (1995) found an interstudy variation of 8% for repeated MR studies. Here, our data compare favorably with a mean variability of 1% for computer-assisted quantification of carotid artery cross-sectional area.

Limitations and Future Directions

In the evaluation of test-retest reproducibility, several carotid artery sections were not suitable for semiautomated edge delineation due to image blurring, presumably due to the subject swallowing during MR data acquisition. This is a problem known from clinical MR imaging of structures in the neck, and the only way to prevent image artifacts due to gross motion is to remind the subject to avoid swallowing during data acquisition. Nevertheless, this limitation of the study commemorates that any semiautomated segmentation tool heavily relies on the overall image quality. This is also true for MR images, which must be acquired with high contrast between the various compartments and high signal-to-noise ratio. Similar to the manual analysis approach, exact delineation of the outer vessel boundary in a patient with a large atherosclerotic plaque would be aggravated. Since the algorithm is dependent on the contrast between the low signal from the adventitia and the brighter signal from the surrounding tissue, in patients with significant plaque size the outer border of the vessel wall along the plaque has to be interpolated from the segmentation points in the adjacent area of the plaque with clear adventitial definition.

Measurement of several lumens within one image can be performed by the algorithm by cropping each vessel of interest from the complete MR image and analyzing it separately. Hence, both internal and external carotid arteries can be assessed separately in each slice acquired above the carotid bifurcation. However, measurements of vascular dimensions at the actual site of the bifurcation are not feasible using the semiautomated software, since the vessel circumference is incomplete at this level. Hence, the software cannot provide a correct unwrapping and consequently fails to give a 360° profile of the vessel wall dimensions. Therefore, the image plane encompassing the site of carotid bifurcation has been excluded from data analysis, while the neighboring slices showing the common carotid artery and the internal and external carotid arteries, respectively, were quantitated by the automated method.

Whereas we applied the algorithm only to black blood MR images in the present study, an extension of this method to other MR sequences producing different

contrast features might be feasible. Hence, this algorithm may also work equally well on time-of-flight images with high signal intensity from moving blood (bright blood MRI) and relatively low signal intensity from the vessel wall and the perivascular tissue. Whether such an approach may be advantageous for edge detection based postprocessing has to be determined in further studies.

CONCLUSION

In this study, we demonstrate that semiautomated analysis methods can provide approaches that benefit from the human understanding of the image and the computer's ability to measure precisely and rapidly. Thus, by combining the latest vascular MRI methods and semiautomated image analysis methods, we are now able to reproducibly determine the geometric parameters of blood vessels. This will enable us to follow structural changes in the vessel wall during atherosclerosis progression or regression with high precision, as it has been impressively demonstrated in previous vascular MR studies (Corti et al., 2001, 2002). Hence, this algorithm may be a useful tool in the evaluation of pathophysiologic concepts of arteriosclerosis and novel therapeutic strategies for future studies.

ACKNOWLEDGMENTS

This study was supported by grants from the Chinese Government (QW), from the Wellcome Trust (Intermediate Research Fellowship to FW), the German Academic Exchange Service (SEP), the British Heart Foundation (SN, KC), and the Deutsche Forschungsgemeinschaft (FW).

REFERENCES

- ACAS. (1994). Clinical advisory: carotid endarterectomy for patients with asymptomatic internal carotid artery stenosis. *Stroke* 25:2523–2524.
- Berr, S. S., Hurt, N. S., Ayers, C. R., Snell, J. W., Merickel, M. B. (1995). Assessment of the reliability of the determination of carotid artery lumen sizes by quantitative image processing of magnetic resonance angiograms and images. *Magn. Reson. Imaging* 13:827–835.
- Canny, J. R. A. (1986). Computational approach to edge detection. *IEEE Trans. Pattern Anal. Mach. Intell.* 8:679–698.
- Cao, J. J., Thach, C., Manolio, T. A., Psaty, B. M., Kuller, L. H., Chaves, P. H., Polak, J. F., Sutton-Tyrrell, K., Herrington, D. M., Price, T. R., Cushman, M. (2003). C-reactive protein, carotid intima-media thickness, and incidence of ischemic stroke in the elderly: the cardiovascular health study. *Circulation* 108:166–170.
- Chan, S. K., Jaffer, F. A., Botnar, R. M., Kissinger, K. V., Goepfert, L., Chuang, M. L., O'Donnell, C. J., Levy, D., Manning, W. J. (2001). Scan reproducibility of magnetic resonance imaging assessment of aortic atherosclerosis burden. *J. Cardiovasc. Magn. Reson.* 3:331–338.
- Corti, R., Fayad, Z. A., Fuster, V., Worthley, S. G., Helft, G., Chesebro, J., Mercuri, M., Badimon, J. J. (2001). Effects of lipid-lowering by simvastatin on human atherosclerotic lesions: a longitudinal study by high-resolution, noninvasive magnetic resonance imaging. *Circulation* 104:249–252.
- Corti, R., Fuster, V., Fayad, Z. A., Worthley, S. G., Helft, G., Smith, D., Weinberger, J., Wentzel, J., Mizsei, G., Mercuri, M., Badimon, J. J. (2002). Lipid lowering by simvastatin induces regression of human atherosclerotic lesions: two years' follow-up by high-resolution noninvasive magnetic resonance imaging. *Circulation* 106:2884–2887.
- Fayad, Z. A., Nahar, T., Fallon, J. T., Goldman, M., Aguinaldo, J. G., Badimon, J. J., Shinnar, M., Chesebro, J. H., Fuster, V. (2000a). In vivo magnetic resonance evaluation of atherosclerotic plaques in the human thoracic aorta: a comparison with transesophageal echocardiography. *Circulation* 101:2503–2509.
- Fayad, Z. A., Fuster, V., Fallon, J. T., Jayasundera, T., Worthley, S. G., Helft, G., Aguinaldo, J. G., Badimon, J. J., Sharma, S. K. (2000b). Noninvasive in vivo human coronary artery lumen and wall imaging using black-blood magnetic resonance imaging. *Circulation* 102:506–510.
- Feng, J., Lin, W. C., Chen, C. T. (1991). Epicardial boundary detection using fuzzy reasoning. *IEEE Trans. Med. Imaging* 10:187–199.
- Glagov, S., Weisenberg, E., Zarins, C. K., Stankunavicius, R., Kolettis, G. J. (1987). Compensatory enlargement of human atherosclerotic coronary arteries. *N. Engl. J. Med.* 316:1371–1375.
- Kass, M., Witkin, A., Terzopoulos, D. (1988). Snakes: active contour models. *Int. J. Comput. Vis.* 4:321–331.

- Klingler, J. W., Jr., Vaughan, C. L., Fraker, T. D., Jr., Andrews, L. T. (1988). Segmentation of echocardiographic images using mathematical morphology. *IEEE Trans. Biomed. Eng.* 35:925–934.
- Li, A. E., Kamel, I., Rando, F., Anderson, M., Kumbasar, B., Lima, J. A., Bluemke, D. A. (2004). Using MRI to assess aortic wall thickness in the multiethnic study of atherosclerosis: distribution by race, sex, and age. *AJR Am. J. Roentgenol.* 182:593–597.
- Melton, H. E., Jr., Collins, S. M., Skorton, D. J. (1983). Automatic real-time endocardial edge detection in two-dimensional echocardiography. *Ultrasound Imag.* 5:300–307.
- Montauban van Swijndregt, A. D., De Lange, E. E., De Groot, E., Ackerstaff, R. G. (1999). An in vivo evaluation of the reproducibility of intima-media thickness measurements of the carotid artery segments using B-mode ultrasound. *Ultrasound Med. Biol.* 25:323–330.
- North American Symptomatic Carotid Endarterectomy Trial Collaborators. (1991). Beneficial effect of carotid endarterectomy in symptomatic patients with high-grade carotid stenosis. *N. Engl. J. Med.* 325:445–453.
- Rewis, D., Panse, N., Sasseen, B., Bass, T., Costa, M. (2003). Differentiation between ruptured plaque and vulnerable plaque using IVUS color flow. *Int. J. Cardiovasc. Interv.* 5:212.
- Ross, R. (1999). Atherosclerosis—an inflammatory disease. *N. Engl. J. Med.* 340:115–126.
- Sahara, M., Kirigaya, H., Oikawa, Y., Yajima, J., Ogasawara, K., Satoh, H., Nagashima, K., Hara, H., Nakatsu, Y., Aizawa, T. (2003). Arterial remodeling patterns before intervention predict diffuse in-stent restenosis: an intravascular ultrasound study. *J. Am. Coll. Cardiol.* 42:1731–1738.
- Shinnar, M., Fallon, J. T., Wehrli, S., Levin, M., Dalmacy, D., Fayad, Z. A., Badimon, J. J., Harrington, M., Harrington, E., Fuster, V. (1999). The diagnostic accuracy of ex vivo MRI for human atherosclerotic plaque characterization. *Arterioscler. Thromb. Vasc. Biol.* 19:2756–2761.
- Toussaint, J. F., LaMuraglia, G. M., Southern, J. F., Fuster, V., Kantor, H. L. (1996). Magnetic resonance images lipid, fibrous, calcified, hemorrhagic, and thrombotic components of human atherosclerosis in vivo. *Circulation* 94:932–938.
- Weiss, C. R., Arai, A. E., Bui, M. N., Agyeman, K. O., Waclawiw, M. A., Balaban, R. S., Cannon, R. O., III. (2001). Arterial wall MRI characteristics are associated with elevated serum markers of inflammation in humans. *J. Magn. Reson. Imaging* 14:698–704.
- Wu, Z., McMillan, T. L., Mintz, G. S., Maehara, A., Canos, D., Bui, A. B., Waksman, R., Weissman, N. J. (2003). Impact of the acute results on the long-term outcome after the treatment of in-stent restenosis: a serial intravascular ultrasound study. *Catheter. Cardiovasc. Interv.* 60:483–488.
- Yuan, C., Beach, K. W., Smith, L. H., Jr., Hatsukami, T. S. (1998). Measurement of atherosclerotic carotid plaque size in vivo using high resolution magnetic resonance imaging. *Circulation* 98:2666–2671.
- Yuan, C., Lin, E., Millard, J., Hwang, J. N. (1999). Closed contour edge detection of blood vessel lumen and outer wall boundaries in black-blood MR images. *Magn. Reson. Imaging* 17:257–266.
- Yuan, C., Mitsumori, L. M., Beach, K. W., Maravilla, K. R. (2001). Carotid atherosclerotic plaque: non-invasive MR characterization and identification of vulnerable lesions. *Radiology* 221:285–299.
- Zhang, L. F., Geiser, E. A. (1984). An effective algorithm for extracting serial endocardial borders from 2-dimensional echocardiograms. *IEEE Trans. Biomed. Eng.* 31:441–447.
- Zhang, S., Hatsukami, T. S., Polissar, N. L., Han, C., Yuan, C. (2001). Comparison of carotid vessel wall area measurements using three different contrast-weighted black blood MR imaging techniques. *Magn. Reson. Imaging* 19:795–802.
- Zhang, S., Cai, J., Luo, Y., Han, C., Polissar, N. L., Hatsukami, T. S., Yuan, C. (2003). Measurement of carotid wall volume and maximum area with contrast-enhanced 3D MR imaging: initial observations. *Radiology* 228:200–205.

Submitted February 24, 2004

Accepted July 2, 2004